RSC Advances

High Pressure Structures and Superconductivity of AlH3 (H2) Predicted by First Principles

Journal:	*RSC Advances*
Manuscript ID:	RA-ART-11-2014-014990
Article Type:	Paper
Date Submitted by the Author:	21-Nov-2014

Complete List of Authors:	Hou, PuGeng; JiLin university, Zhao, Xiusong; JiLin university, Tian, Fubo; Jilin University, Li, Da; Jilin University, Duan, Defang; JiLin university, State Key Laboratory of Superhard Materials zhao, Zhonglong; Jilin University, Chu, Binhua; Jilin University, Liu, Bingbing; Jilin University, State Key Laboratory of Superhard Materials Cui, Tian; JiLin university, State Key Laboratory of Superhard Materials

High Pressure Structures and Superconductivity of $AlH_3(H_2)$ Predicted by First Principles

Pugeng Hou, Xiusong Zhao, Fubo Tian, Da Li, Defang Duan, Zhonglong Zhao, Binhua Chu, Bingbing Liu and Tian Cui*

State Key Laboratory of Superhard Materials, College of Physics, Jilin University, Changchun 130012, People's Republic of China

Abstract

Motivated by the potential high-temperature superconductivity in hydrogen-rich materials, the high-pressure structures of $AlH_3(H_2)$ in the pressure range of 25–300 GPa were extensively explored by using a genetic algorithm. We found an insulating *P*1 phase, a semiconducting *P*-1 phase and an intriguing sandwich-like metallic phase with space group of $P2_1/m$-*Z* (containing Z shape net layers of Al atoms). We found that the H_2 molecules in the environment of AlH_3 became metallic and showed molecular semi-molecular phenomenon. Applying the Allen-Dynes to modify McMillan equation yields remarkably high superconducting temperatures of 132–146 K at 250 GPa, among the higher values reported so far for phonon-mediated superconductors. In this paper, we reveal a unique superconducting mechanism that the direct interactions between H_2 and AlH_3 at high pressure play a major role in the high superconductivity, while the contribution from H_2 vibration is

minor.

I. Introduction

Hydrogen, the lightest element in the nature, has the very high Debye temperature, which makes it become an underlying high-temperature superconductor according to the BCS theory. Therefore, it has attracted extensive interest in the research of the metallization of hydrogen[1]. Static compression experiments showed that hydrogen is an insulator at room temperature up to at least 342 GPa[2]. Theoretically solid hydrogen can become metallic due to either pressure-induced band overlap of molecular hydrogen or molecular dissociation (molecular-to-monatomic transition).

Ashcroft[3] predicted that certain hydrides would present a high superconducting critical temperature while becoming metallic at lower pressures than pure solid hydrogen. Dense hydrides have become the targets for researchers to study metallization and find high-temperature superconductors, such as AlH_3,[4] Si_2H_6,[5] SiH_4,[6] GeH_4[7] and SnH_4.[8] Recently, Vander Waals H_2-containing compounds have attracted many people's interest. Experiments have unexpectedly revealed that H_2 molecules can interact with hydrides CH_4, SiH_4, H_2O, NH_3BH_3, GeH_4 and H_2S, and even with inert gas Ar, Kr and Xe at readily accessible pressures with the formation of intriguing Vander Waals compounds CH_4-H_2,[9] SiH_4-H_2,[10,11] H_2O-H_2,[12–14] NH_3BH_3-H_2,[15] GeH_4-H_2,[16] H_2S-H_2,[17] Ar-H_2,[18]

Kr-$(H_2)_4$,[19] and Xe-H_2.[20] These H_2-containing compounds are of interest as models for studying metallic hydrogen and hydrides. How H_2 molecules change in hydrides and what contributions H_2 molecules make to metallization are attractive.

As a material proposed for storing hydrogen and promised adding to rocket fuels and high explosives, aluminum hydride have been studied widely.[4, 21-23] In view of the low metallization pressure observed in AlH_3[4], we have focused on the metallization and superconductivity of AlH_3-H_2 by first-principles calculations. Crystal structure prediction was performed by genetic algorithm and electron-phonon coupling (EPC) calculations[24] were performed by linear response theory. Three structures of insulating $P1$ phase, semiconducting $P\text{-}1$ phase and metallic $P2_1/m$-Z phase for $AlH_3(H_2)$ have been predicted. Our calculations revealed that the metallization and remarkably high superconductivity of $AlH_3(H_2)$ at high pressures. Through EPC calculations, we can show that the $P2_1/m$-Z phase emerges remarkably high critical temperatures about 132–146 K at 250 GPa, among the higher values reported for hydrogen-rich compounds to date. The current results suggest a unique superconducting mechanism which is likely to have important implications on other high-pressure H_2-containing compounds.

II. Computational Methods and Details

1. In this paper, we have explored high-pressure structures of AlH_3 (H_2) by using *ab initio* evolutionary algorithm (EA) as implemented in the USPEX (Universal Structure Predictor: Evolutionary Xtallography) code[25-27].This code has been applied successfully to a number of systems[7, 8, 28-32]. The most significant feature of this methodology is the capability of predicting the stable structure only with the knowledge of the chemical composition. The first generation of structures is produced randomly. Each subsequent generation is produced from 60% of the lowest-enthalpy structures of the preceding generation. In addition, the lowest-enthalpy structure always survived into the next generation. The variation operators are used for producing offspring included heredity (60% structures), lattice mutation (20%), and atomic permutation (20%). The underlying structure relaxations were performed using density functional theory within the Perdew-Burke-Ernzerhof (PBE) generalized gradient approximation (GGA) [33], as implemented in the CASTEP code [34]. We carry out a GGA calculation of the isolated alane molecule in vacuum and compare to the G4 (MP2) value[35]. The difference of energy is relatively small. So it will be accurate for choosing GGA method to calculate a periodic structure. The structural optimizations were performed by the Broyden–Fletcher–Goldfarb–Shanno algorithm[36], which provides a fast way of finding the lowest energy structure and the optimized cell. The

optimization was not finished until the forces on the atoms were less than 0.01 eV/Å and all the stress components were less than 0.02 GPa. The norm-conserving scheme[37] was used to generate the pseudo potentials for H and Al with electronic configuration of $1s^1$ and $3s^23p^1$, respectively. Convergence tests adopted the kinetic energy cutoff of 800 eV and the Monkhorst–Pack[38] k-point mesh of 8×8×6, 11×8×7, and 6×6×12 were used for P1, P-1, and $P2_1/m$-Z structures, respectively. Elastic constants were calculated by the strain-stress method. The lattice dynamics and electron-phonon coupling (EPC) [24] calculations were carried out using linear-response theory through the Quantum ESPRESSO package.[39] The kinetic energy cutoff of 90 Ry for $P2_1/m$-Z structure was employed to give a perfect convergence. The q-point mesh in the first BZ of 4×4×8 for $P2_1/m$-Z structure was adopted in the interpolation of the force constants for the phonon dispersion curve calculations. A denser 8×8×16 k-point mesh for $P2_1/m$-Z structure was used to ensure k-point sampling convergence with Gaussians of width 0.04 Ry, which approximates the zero width limits in the calculation of EPC parameter λ.

III. Results and Discussion

We performed evolutionary variable-cell structure prediction simulations from one to six AlH5 formula units (f. u.) per cell at 10, 30, 50, 100, 150, 200, 250, and 300 GPa. Through the analysis of the result, we found that there are three stable structures under this pressure region: triclinic *P*1 (6 f. u./cell) at 10, 30 and 50 GPa, triclinic *P*-1 (4 f.u./cell) at 100 and 150 GPa, and monoclinic $P2_1/m$-*Z* (4 f. u./cell) at 200, 250, and 300 GPa, as is depicted in Fig. 1, and the parameters and atomic positions are listed in table 1. It is also very interesting to determine what other meta-stable structures are in AlH5 under high pressure.

In the shortlist of the other candidates, the structures with covalent bond between H and AlH_4 are less stable than the structures containing unit "H2", liked hydrogen molecule. The enthalpy curves of the selected structures as a function of pressure indicate that Vander Waals compounds AlH_3-H_2 is energetically more favorable than other formations like *Cmcm* and *Imm*2 structures. Furthermore, to study AlH_3:H_2 ratio in Vander Waals compounds AlH_3-H_2, we also explored AlH_7 (1:2 AlH_3:H_2) and AlH_9 (1:3 AlH_3:H_2) with method as AlH_5 (1:1 AlH_3:H_2). Enthalpy calculations (Fig. 2) show that $AlH_3(H_2)$ is easier to be synthesized than $AlH_3(H_2)_2$ and $AlH_3(H_2)_3$. Moreover, in order to investigate the stability of all structures in $AlH_3(H_2)_2$ under certain pressure, we have examined whether it decomposes into Al and H2. We

took the face-centered cubic structure for Al and the *Pa*-3 structure for H_2 which is phase I of solid hydrogen[40]. Combining the data with our results for AlH_5 (Fig. 2), we determined that the *P*1, *P*-1 and $P2_1/m$-*Z* phases are stable. At 10 GPa, our calculations have predicted two structures with space groups *Pccm* (2 f.u./cell) and P1. Any Al atom and its neighboring H atoms evolve into corner-shared AlH_6 octahedra which is the same as AlH_3 at low pressure, while H_2 molecules occupy the interstitial sites among AlH_6 octahedras. Calculations show that H-H bond lengths of H_2 molecules derived from the more stable P1 structure (Fig. 1a) at 30 GPa are 0.745 and 0.752 Å, slightly longer than that (0.737 Å) in pure solid H_2[42].

At 73 GPa, the *P*1 structure transforms to *P*-1 structure (Fig. 1b). This new structure starts to show sandwich-like structure while H_2 molecules are distributed in interlayer between the AlH_3 layers. It is a transitional structure to $P2_1/m$-*Z* space group. The *P*-1 structure is a semiconductor and stable up to 250 GPa, above which the $P2_1/m$-*Z* structure (Fig. 1c) is more stable. The framework of Al in this structure shows Z shape net in the sandwich-like layer. So we called it $P2_1/m$-*Z* structure to distinguish it from the $P2_1/m$-*W* structure (W shape) which is also found with USPEX code. Interestingly the intra-molecular H-H bond was significantly stretched to be 0.838 Å and 0.803 Å at 250 GPa. And obviously, it is much longer than that in pure solid H_2[39]. The elongation

of H-H bonds might be mainly resulted from the continuously increased AlH_3-H_2 interactions under pressure.

The mechanical stability of structure provides a useful insight into the stability of crystals. The strain energy of a crystal must be positive against any homogeneous elastic deformations, i.e., the matrix of elastic constants C_{ij} must be positive definite[38]. It should note that negative values are not prohibited for C_{ij}[40]. To evaluate the mechanical stability of the three phases, elastic constants have been calculated and listed in Table II. Obviously, the elastic constants of the three structures satisfy the mechanical stability criteria[41, 42] indicating that the three structures are mechanically stable.

The band gap of the P1 and P-1 structure are calculated to be 3.15 eV and 1.45 eV at 25 GPa and 150 GPa, respectively. It reveals that P1 structure is an insulator while *P*-1 structure is a semiconductor. At 250 GPa, the *P*-1 structure transforms to $P2_1/m$-*Z* structure. The electronic band structure and projected DOS for the $P2_1/m$-*Z* structure show that it is a metal phase with a large DOS at Fermi level (1.20 states/eV/unit cell) (Fig. 3c and 3d). The projected DOS clearly indicates strong hybridizations of Al, H_1 (H atom in AlH_3) and H_2 (H atom in H_2) orbital. This hybridization results in a 25.4 eV wide valence band favorable to become a good superconductor, in accordance with the previous predictions for dense hydrogen alloys.[3] Phonon dispersion curves for *P*1,

P-1 and $P2_1/m$-*Z* structure have been calculated as shown in Fig. 4. The absence of any imaginary frequency suggests that the three structures are dynamical stable. For the $P2_1/m$-*Z* structure, the low frequency bands below 13 THz and high energy bands above 90 THz are dominated by Al vibrations and H_2 vibration, respectively. It is noteworthy that strong coupling of Al-H2 (13–22 THz) and H1-H2 (22–81 THz) vibrations is revealed and largely contrasted to the clear separation of frequency regions found in SiH_4, GeH_4, and SnH_4[6-8]. The strong covalent interactions between AlH_3 and H_2 molecules are playing an important role in this phenomenon.

The phonon density of states (Fig. 5a), Eliashberg spectral function $\alpha^2F(\omega)$ and the EPC parameter λ of the $P2_1/m$-*Z* structure (Fig. 5b) as a function of frequency at 250 GPa are calculated to explore the possible superconductivity of $AlH_3(H_2)$. The resulting total λ[43] is 1.625 indicating that the EPC is extremely strong. The logarithmic average frequency ω_{log}[44] is 949 K which is calculated directly from the phonon spectrum. The Coulomb pseudo-potential μ^* is often taken as 0.1 for most metals, an appropriate one proposed by Ashcroft[3] is 0.13 for hydrogen dominant metallic alloys. By applying ω_{log} (949 K) into the Allen and Dynes modified McMillan equation[44] with the typical choice of μ^* as 0.1–0.13, a remarkable large T_c in the range of 132–146 K was derived. The current results support the earlier theoretical proposal that hydrogen dominant

metallic alloys are high-temperature superconductors[3]. However, the T_c magnitude of 132-146 K strikingly achieved from $AlH_3(H_2)$ is the higher values among all previously reported hydrides[6-8,45]. This result invites us to probe the underlying superconducting mechanism originated from the additional H_2 molecules. We then decomposed the total λ into several major individual contributions. The low frequency Al translational vibrations (below 13 THz) were found to contribute 28% in total. It is regretful to find that H2 vibration (>90 THz) contributes only 2% of λ. Instead, a remarkable feature prompts to us that the H_2-AlH_3 coupling (13–90 THz) constitutes 70% of the total λ. This result highlights the significant role played by H_2 molecules in the superconductivity through the strong interactions with AlH_3 molecules enhancing the attractive EPC over the repulsive Coulomb interaction between electrons. This physical mechanism apparently contrasted to those in high-pressure GeH_4[7] and SnH_4[8], where the semi-molecular H-H vibrations dominate the superconductivity.

IV. Conclusion

We have extensively explored the high-pressure crystal structures of AlH_3-H_2 by *ab initio* first-principle calculations. The evolutionary algorithm was used for structural prediction. Three structures of insulating *P*1 phase, semiconducting *P*-1 phase and metallic $P2_1/m$-*Z* phase for $AlH_3(H_2)$ have been found. Enthalpy curves, elastic constants and lattice dynamics calculations show that the three structures are thermodynamically, mechanically, and dynamically stable, respectively. By the use of EPC calculations we acquired the remarkably high critical temperatures of 132–146 K for the $P2_1/m$-*Z* phase 250 GPa, among the higher values reported for hydrogen-rich compounds to date. The current results reveal a unique superconducting mechanism with the strong interactions between H_2 and AlH_3 dominating the superconductivity of $AlH_3(H_2)$.

Acknowledgments

We are thankful for the financial support from the National Basic Research Program of China (No. 2011CB808200), Program for Changjiang Scholars and Innovative Research Team in University (No. IRT1132), National Natural Science Foundation of China (Nos. 11074090, 51032001, 11104102, 11404134, 10979001, 51025206, 11204100), National Found for Fostering Talents of basic Science (No. J1103202), Specialized Research Fund for the Doctoral Program of Higher Education (20110061120007, 20120061120008), and China Postdoctoral Science Foundation (2014M561279). Parts of calculations were performed in the High Performance Computing Center (HPCC) of Jilin University.

Notes and references

1 Babaev, E.; Sudbø, A.; Ashcroft, N. W. Nature 2004, **431**, 666 .

2 Loubeyre, P.; Occelli, F.; Letoullec, R. Nature 2002, **416**, 613.

3 Ashcroft N.W. Phys. Rev. Lett. 2004, **92**, 187002.

4 Goncharenko, I.; Eremets, M.I.; Hanfland, M.; Tse, J.S. Phys. Rev. Lett. 2008, **100**, 045504.

5 Jin, X.; Meng, X.; He, Z. Proc. Natl. Acad. Sci. 2010, **107**, 9969–9973.

6 Eremets, M.I. Science 2008, **319**, 1506–1509.

7 Gao,G. Y.; Oganov, A. R. Phys. Rev.Lett. 2008, **101**, 107002.

8 Gao, G. Y.; Oganov, A. R.; Li, P.f. Proc. Natl. Acad. Sci. 2010, **107**, 1317–1320.

9 Somayazulu, M. S.; Finger, L. W.; Hemley, R. J.; Mao, H. K. Science 1996, **271**, 1400.

10 Wang, S.; Mao, H.; Chen, X. J.; Mao, W. L. Proc. Natl. Acad. Sci. U.S.A. 2009, **106**, 14763.

11 Strobel, T. A.; Somayazulu, M.; Hemley, R. J. Phys. Rev.Lett. 2009, **103**, 065701.

12 Mao, W. L.; Mao, H. Proc. Natl. Acad. Sci. U.S.A. 2004, **101**, 708.

13 Mao, W. L.; Mao, H.; Goncharov, A. F.; Struzhkin, V. V. Science 2002, **297**, 2247.

14 Vos, W. L.; Finger, L. W.; Hemley, R. J.; Mao, H.-K. Phys.Rev. Lett. 1993, **71**, 3150.

15 Lin, Y.; Mao, W. L.; Proc. Natl. Acad. Sci. U.S.A. 2009, **106**, 8113.

16 Strobel, T A.; Chen, X. J.; Somayazulu, M.; Hemley, R. J.; J. Chem. Phys. 2010, **133**,164512.

17 Strobel, T A.; Somayazulu, M.; Hemley, R. J.; Phys. Rev. Lett. 2011, **107**, 255503.

18 Loubeyre, P.; Letoullec, R.; Pinceaux, J. P. Phys. Rev. Lett. 1994, **72**, 1360.

19 Kleppe, A. K.; Amboage, M.; Jephcoat, A. P.; Sci. Rep. 2014, **4**, 4989.

20 Somayazulu, M.; Dera, P.; Goncharov, A. F.; Gramsch, S. A. Nat. Chem. 2010, **2**, 50.

21 Pickard, C. J.; Needs, R. J. Phys. Rev. B 2007, **76**, 144114.

22 Kim, D. Y.; Scheicher, R. H. Ahuja, R. Phys. Rev. B 2008, **78**, 100102.

23 Wang, Y.; Yan, J. A.; Chou, M. Y. Phys. Rev. B 2008, **77**, 014101.

24 Allen, P. B. Phys. Rev. B 1972, **6**, 2577.

25 Oganov, A. R.; Lyakhov, A. O.; Valle, M. Acc. Chem. Res. 2011, **44**, 227-237.

26 Oganov, A.R.; Glass, C.W. J. Chem. Phys. 2006, **124**,244704.

27 Glass, C. W.; Oganov, A. R.; Hansen, N. Comput Phys Commun 2006, **175**, 713–720.

28 Oganov, A. R. Nature 2009, **457**, 863–867.

29 Ma, Y.; Eremets, M.I.; Oganov, A. R. Nature 2009, **458**, 182-185.

30 Zhu, Q.; Oganov, A. R.; Salvado, M.; Pertierra, P. Phys. Rev. B 2011, **83**, 193410.

31 Wen, X. D.; Hand, L.; Labet, V.; Yang, T.; Hoffmann, R.; Ashcroft, N.W.; Oganov, A. R. Proc. Natl. Acad. Sci. 2011, **108**, 6833-6837.

32 Zurek, E.; Hoffmann, R.; Ashcroft, N. W.; Oganov, A. R.; Lyakhov, A. O. Proc. Natl. Acad. Sci. 2009, **106**, 17640-17643.

33 Perdew, J. P.; Burke, K.; Ernzerhof, M. Phys. Rev. Lett. 1996, **77**, 3865–3868.

34 Segall, M. D.; Lindan, P. J. D.; Probert, M. J.; Pickard, C. J.; Hasnip, P. J.; Clark, S.J.; Payne, M. C. J. Phys.: Condens. Mat. 2002, **14**, 2717.

35 Wong, B. M.; Lacina, D.; Nielsen,I. M. B.; Graetz, J.; Allendorf, M. D. J. Phys. Chem. C, 2011 115, 7778.

36 Pfrommer, B. G.; Côté, M.; Louie, S. G.; Cohen, M. L. J. Comput. Phys. 1997, **131**, 233.

37 Troullier, N.; Martins, J. L. Phys. Rev. B 1991, **43**, 1993.

38 Monkhorst, H. J.; Pack, J. D. Phys. Rev. B 1976, **13**, 5188.

39 Scandolo, S.; Giannozzi, P.; Cavazzoni, C. Z. Kristallogr. 2005, **220**, 574–579.

40 Pickard, C. J.; Needs, R. J. Nat. Phys. 2007, **3**, 473–476.

41 Kresse, G.; Furthmüller, J. Phys. Rev. B 1996, **54**, 11169–11186.

42 John, P.;Kieron, B.;Matthias,E. Phys. Rev. Lett. 1996, **77**, 3865–3868.

43 Allen, P. B.; Dynes, R. C. Phys. Rev. B 1975, **12**, 905–922.

44 Baroni Stefano http://www.pwscf.org/.

45 Wang, H.; Tse, J. S.; Ma, Y. Proc. Natl. Acad. Sci. 2012, **109**, 6463-6466.

Tables and Figures

Table I Structure parameters of our predicted *P*1, *P*-1 and $P2_1/m$-*Z* structures of AlH_3 (H_2) at high pressures. H1 and H2 in the table represent the H atoms in the AlH_3 and H_2 molecules, respectively.

Table II Elastic constants C_{ij} (GPa) of P1, P-1 and $P2_1$/m-Z structures calculated at 30, 150 and 250 GPa, respectively.

Fig. 1 The crystal structures of (a) the P1 structure at 25 GPa, (b) the P-1 structure at 150 GPa and (c) the P21/m-Z structure at 250 GPa.

Fig. 2 Calculated enthalpy curves for various structures relative to our predicted *P*-1 structure as a function of pressure. The decomposition enthalpy into Al + $5/2H_2$ was plotted (black dash line). We also compare the enthalpies of AlH_7 and AlH_9 (shot dot line) with AlH_5, structures of *P*1 at 10–30 GPa, and $P2_1$/m at 30-300 GPa for AlH_7, P2/c at 10–35 GPa and *P*-1 at 35–300 GPa for AlH_9, *Pa*-3 at 0–100 GPa and *C*2/*c* at 100–250 GPa and *Cmca* above 250 GPa for H_2 are adopted.

Fig. 3 (a) and (b) The calculated electronic band structures for P1 structure at 25 GPa and P-1 structure at 150 GPa. (c) and (d) the electronic band structure and projected DOS of the $P2_1$/m-Z structure at 250 GPa.

Fig. 4 Calculated phonon dispersion curves for $AlH_3(H_2)$ with P1 structure at 25 GPa (a), P-1 structure at 150 GPa (b) and $P2_1$/m-Z structure at 250 GPa (c).

Fig. 5 Calculated phonon density of states (PHDOS) (a) and the Eliashberg phonon spectral function α^2F (ω) and electron phonon integral λ (ω) (b) for the P21/m-Z structure at 250 GPa.

Table I

Space group	P1	Lattice parameters (Å)					
Pressure	25 GPa	a	b	c	α	β	γ
Atomic coordinates		4.3140	4.4684	5.4130	77.3848	75.8524	74.3170
Al	(0.4352,0.3944,0.1688)			Al	(0.0026,0.9590,0.3667)		
Al	(0.8628,0.8185,0.9896)			H1	(0.1163,0.0132,0.0393)		
H1	(0.1255,0.4793,0.0198)			H1	(0.2697,0.1405,0.3836)		
H1	(0.7322,0.2973,0.3396)			H1	(0.2897,0.6379,0.3711)		
H1	(0.7410,0.7651,0.3238)			H1	(0.9699,0.8849,0.6779)		
H1	(0.6029,0.6432,0.9461)			H1	(0.5829,0.1476,0.9637)		
H2	(0.4417,0.0198,0.6150)			H2	(0.4152,0.9860,0.7598)		
H2	(0.4771,0.5863,0.6431)			H2	(0.4916,0.4144,0.6877)		
H2	(0.9307,0.4049,0.6472)			H2	(0.0529,0.3474,0.7332)		
Space group	P-1	Lattice parameters (Å)					
Pressure	150 GPa	a	b	c	α	β	γ
Atomic coordinates		3.2749	4.3164	5.5170	107.748	99.7819	98.3688
Al	(0.2560,0.8383,0.7951)			Al	(0.3416,0.2689,0.5657)		
H1	(0.5862,0.7725,0.0190)			H1	(0.4268,0.9651,0.3214)		
H1	(0.9984,0.9469,0.3401)			H1	(0.8254,0.5258,0.1999)		
H1	(0.2727,0.3090,0.2735)			H1	(0.8244,0.3531,0.5176)		
H2	(0.0466,0.2042,0.9691)			H2	(0.8126,0.1017,0.8999)		
H2	(0.6329,0.4320,0.9089)			H2	(0.8199,0.4314,0.8396)		
Space group	$P2_1/m$	Lattice parameters (Å)					
Pressure	250 GPa	a	b	c	α	β	γ
Atomic coordinates		5.2145	2.5553	4.6144	90.0000	75.5215	90.0000
Al	(0.1963,0.7500,0.4923)			Al	(0.2174,0.2500,0.9461)		
H1	(0.2162,0.7500,0.1411)			H1	(0.1018,0.2500,0.3333)		
H1	(0.4075,0.2500,0.4491)			H1	(0.0820,0.2500,0.6888)		
H1	(0.0546,0.7500,0.8660)			H1	(0.3568,0.7500,0.7290)		
H2	(0.4868,0.2500,0.0727)			H2	(0.3711,0.2500,0.2325)		
H2	(0.4713,0.2500,0.6517)			H2	(0.5369,0.2500,0.7910)		

Table II

P1	C_{11}	C_{22}	C_{33}	C_{44}	C_{55}	C_{66}	C_{12}	C_{13}	C_{14}	C_{15}
30 GPa	150.4	116.4	113.1	47.4	34.5	39.0	37.9	40.1	3.6	-3.8
C_{16}	C_{23}	C_{24}	C_{25}	C_{26}	C_{34}	C_{35}	C_{36}	C_{45}	C_{46}	C_{56}
-4.7	51.9	-11.7	8.3	-16.2	-2.6	-9.3	10.8	3.2	-2.5	-5.0
P-1	C_{11}	C_{22}	C_{33}	C_{44}	C_{55}	C_{66}	C_{12}	C_{13}	C_{14}	C_{15}
150GPa	774.8	730.6	752.6	169.1	222.4	114.2	400.4	354.8	-9.4	-20.6
C_{16}	C_{23}	C_{24}	C_{25}	C_{26}	C_{34}	C_{35}	C_{36}	C_{45}	C_{46}	C_{56}
23.8	368.1	43.3	9.2	-71.2	-25.7	38.2	24.7	28.1	0.8	1.5
$P2_1/m$	C_{11}	C_{22}	C_{33}	C_{44}	C_{55}	C_{66}				
250GPa	1176.5	1194.9	1195.1	249.4	192.3	235.1				
C_{12}	C_{13}	C_{15}	C_{23}	C_{25}	C_{35}	C_{46}				
597.7	551.7	-71.1	562.1	-82.0	136.5	-19.1				

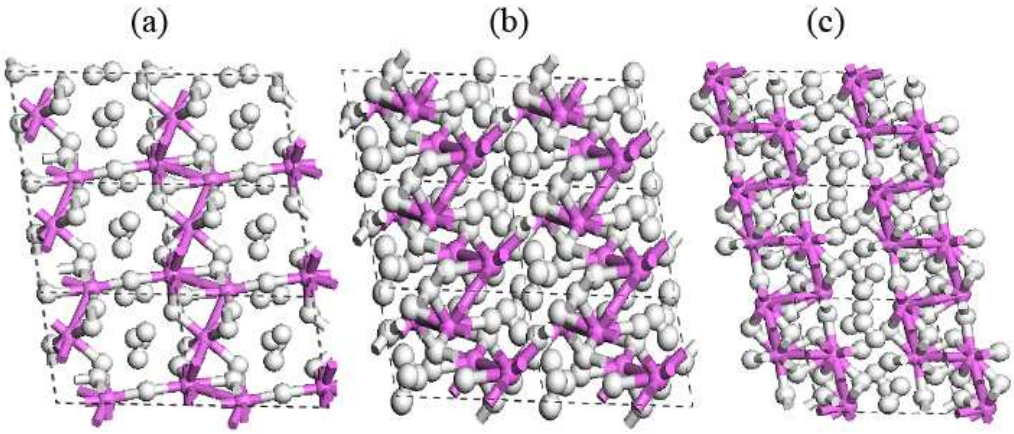

Fig. 1

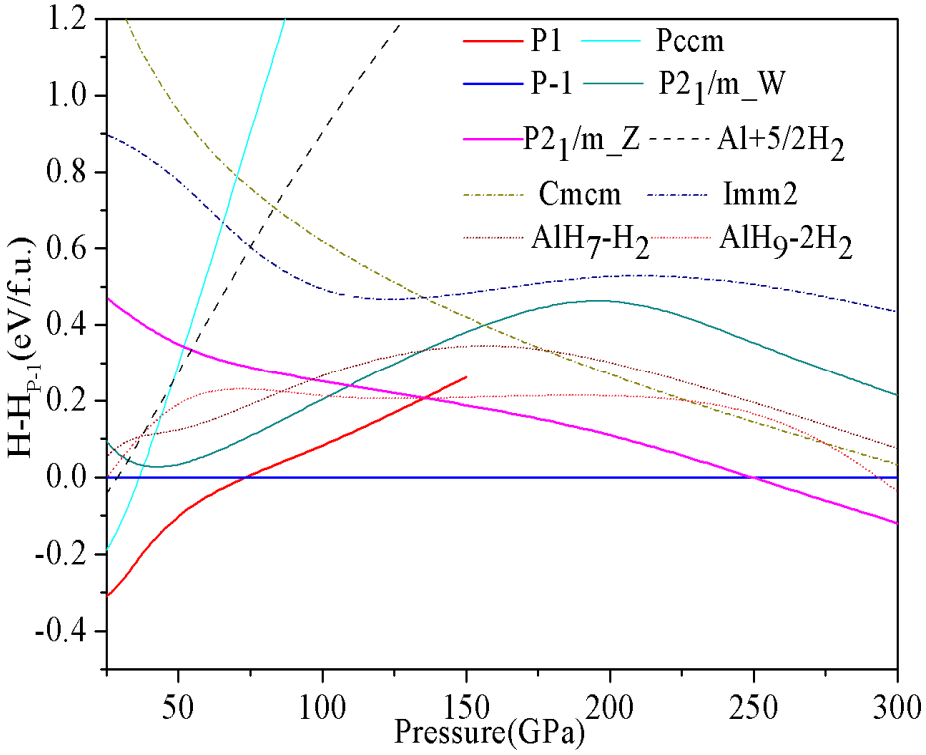
1.2
1.0
0.8
0.6
0.4
0.2
0.0
-0.2
-0.4
H-H$_{P-1}$(eV/f.u.)
50
100
150
200
250
300
Pressure(GPa)
P1
Pccm
P-1
P2$_1$/m_W
P2$_1$/m_Z
Al+5/2H$_2$
Cmcm
Imm2
AlH$_7$-H$_2$
AlH$_9$-2H$_2$

Fig. 2

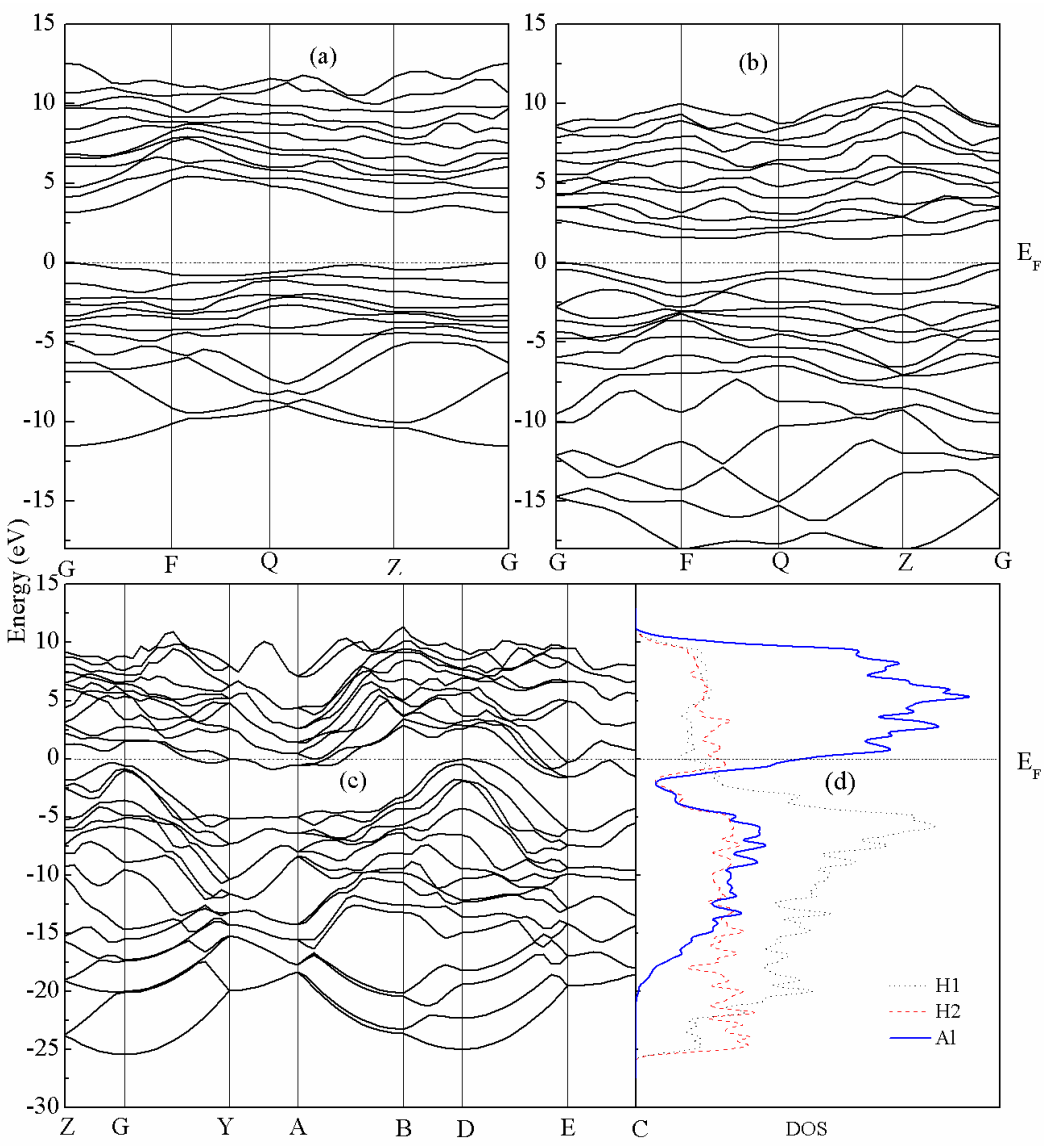

Fig. 3

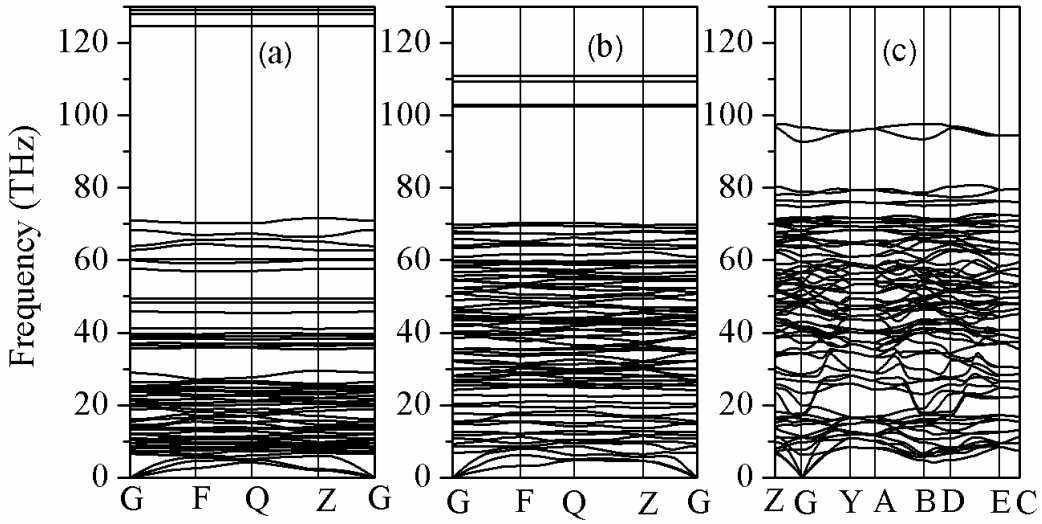

Fig. 4

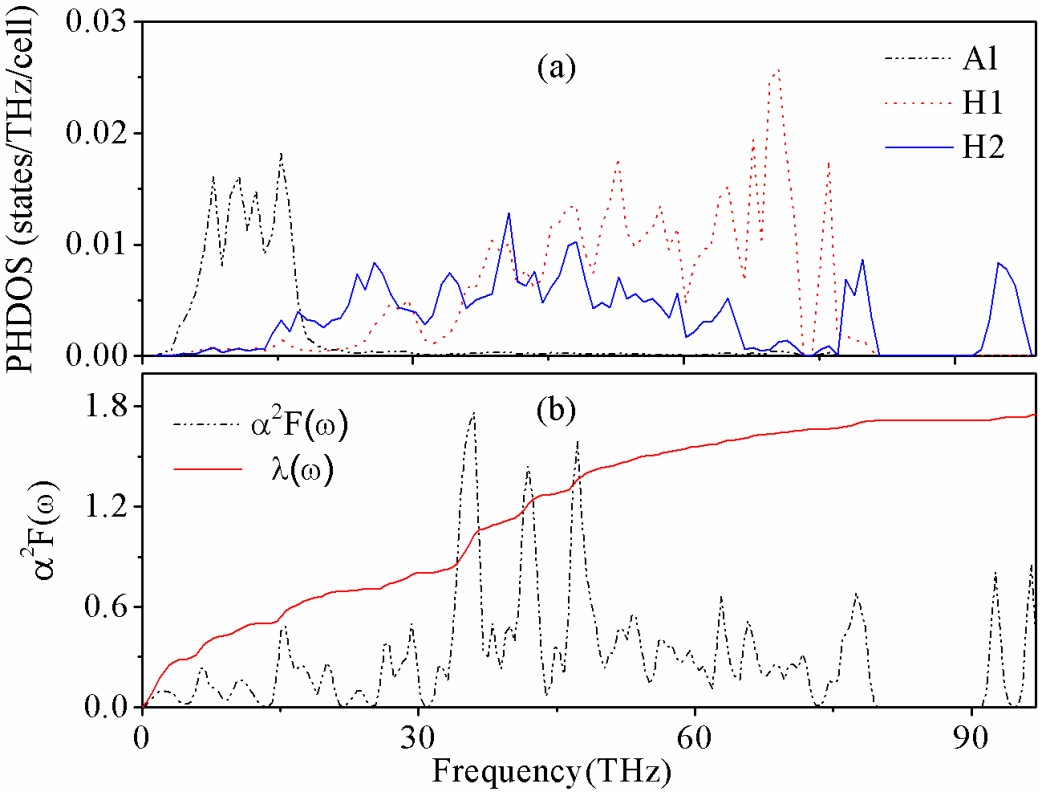
PHDOS (states/THz/cell)
0.03
0.02
0.01
0.00
(a)
Al
H1
H2
1.8
1.2
0.6
0.0
α²F(ω)
(b)
α²F(ω)
λ(ω)
0
30
60
90
Frequency (THz)

Fig. 5